2013 IEEE/RSJ International Conference on
Intelligent Robots and Systems (IROS)
November 3-7, 2013. Tokyo, Japan

A large-area tactile force sensor for measuring ground reaction forces from small legged robots

Shivam S. Desai†, Asa M. Eckert-Erdheim†, and Aaron M. Hoover⋆

Abstract— **This work presents the design, fabrication, calibration, and testing of a multi-touch force sensor designed to measure normal ground reaction forces generated by high-speed locomotion of milli-scale legged robots. The sensor is based on the optical principle of frustrated total internal reflection (FTIR) and is capable of resolving multiple simultaneous normal forces in the range of 50 - 1000 mN at a rate of 250 Hz with measurement error of less than 1%. The sensor is integrated with commercial, off-the-shelf motion capture hardware and the whole system is demonstrated with a simple experiment tracking a bouncing ball and simultaneously recording kinematic state and ground reaction force data.**

I. INTRODUCTION

Recent advances in milli- and micro-scale manufacturing processes have enabled the design and fabrication of highly dynamic, power-autonomous legged robots at very small scales [1]–[4]. Because of their small size and high power density, these robots are capable of dynamic maneuvers that are not possible at larger size scales. Robots like DASH [3] can perform inversion maneuvers similar to cockroaches and geckos [5]; the dynaRoACH robot is capable of running on fluidizing ground [6] where larger robots fail [7]; and the CLASH robot [8] can dynamically climb near-vertical surfaces without the assistance of mechanical engagement mechanisms like claws.

Developing a principled understanding of the dynamics underlying advanced locomotion capabilities like those demonstrated by these robots requires not only high-fidelity kinematic state information, but also information about the reaction forces generated by a robot's interaction with its environment. The small size of these robots presents a significant challenge for the characterization of their locomotion. Conventional robots with masses on the order of hundreds of grams or kilograms and sizes on the order of tens of centimeters can be outfitted with sensor suites that enable full dynamic characterization. For example, encoders, joint torque, pressure, and force sensors are commonly found in larger bio-inspired robots like RHex [9] or RiSE [10]. However, in the cases of the milli-scale robots mentioned above, the sensors themselves may weigh orders of magnitude more than the entire robot.

The use of force plates to measure ground reaction forces is common in biomechanics. In 1938, Manter published a design for the first force plate, which was used to study locomotion of cats [11], and biologists have been using conceptually similar apparatuses ever since. However, force plates cannot inherently resolve individual forces from, for example, simultaneous ground contacts of the feet of a multilegged organism. Efforts to resolve individual ground reaction forces have used different techniques including optical birefringence [12], [13] and arrays of individual strain sensing elements [14]. Optical birefringence can be difficult to work with, and the image processing required to extract force data makes it challenging to implement in realtime. Strain sensing arrays enable measurement of multiple 3D forces but suffer from limited spatial resolution.

By contrast, this work takes inspiration from the domain

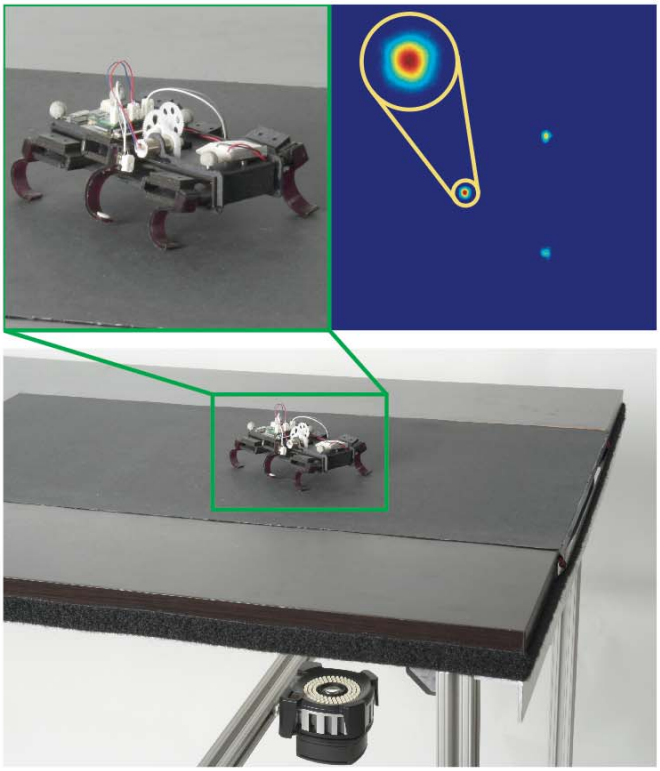

Fig. 1. Above (inset, left), the 24-g dynaRoACH robot sits atop the compliant layer of the force sensor in a tripod stance. The image on the right depicts the three resulting ground reaction forces detected in realtime by the sensor (inset magnified to show detail). Below, the compliant silicone layer can be seen embedded in a tabletop. The blackout skirt has been removed from the area beneath to show the high-speed camera used to capture images of the "frustrated" light that results from applying forces to the surface of the sensor.

†These authors are undergraduates at Olin College of Engineering and contributed equally to this work. Shivam@students.olin.edu, Asa@students.olin.edu

⋆Aaron Hoover is an Assistant Professor of Mechanical Engineering at Olin College of Engineering - aaron.hoover@olin.edu

of tactile sensing and multi-touch user interfaces. Previous multi-touch or tactile force sensors have typically made use of either capacitive [15] or resistive [16] arrays. A standard configuration consists of strip-like conductive electrodes separated by a compliant dielectric (in the case of a capacitive sensor) or a resistive layer coated with a force sensitive resistive ink (in the case of a resistive sensor). Resistive and capacitive tactile sensors are compact, but proper scaling to cover large areas can be difficult and capacitive sensors, in particular, can be prone to noise.

The increasing availability of high-resolution, high-speed cameras has made optical sensing an attractive alternative to the previously mentioned approaches. Recent work in this area has enabled new user interfaces capable of multi-touch, pressure-sensitive interactions [17], [18] using the principle of frustrated total internal reflection (FTIR). Optical FTIR methods have the advantage that spatial resolution is only limited by the CCD of the camera, so a high spatial resolution can be achieved over a relatively large area. For capturing and characterizing ground reaction forces generated by small legged robots, FTIR-based optical methods have the added advantage of being easily integrated with commercially available, multi-camera motion capture systems [19], [20] that rely on imaging infrared light reflected off of passive markers attached to rigid bodies.

The goal of this work is to enable more complete dynamic characterization of small legged robots (like the one pictured in Fig. 1) through the simultaneous measurement of normal ground reaction forces and kinematic state data. To that end, this work details the design, fabrication, and calibration of a multi-touch FTIR force sensor with the significant advantage of being directly integrated with a commercial, off-the-shelf motion capture system to provide synchronized normal ground reaction force and rigid body kinematic state estimates. We present the mechanical design of the sensor and experimental data supporting materials selection and design choices. Using an automated dynamic robotic calibration system, we apply known forces over the active area of the sensor to calibrate out spatial variation and create a map from pixels detected in an image to applied normal force. We conclude with a simple experiment in which a rigid ball is bounced on the sensor, demonstrating the feasibility of integrating force sensing with motion capture.

II. SENSOR DESIGN

A. Principle of Operation

Similar to the multi-touch sensor developed by Han [17], our design utilizes the principle of FTIR [21]. Light traveling in a medium for which the index of refraction (n_1) is much higher than that of the surrounding medium (n_2) will be totally internally reflected if the angle of incidence exceeds the critical angle. However, if a third medium with an index of refraction (n_3) close to n_1 is brought into sufficiently close contact with the first medium, the internal reflection is "frustrated," allowing light to penetrate the second medium.

In order to create the behavior described above, we used the following three media: acrylic (n_1), air (n_2), and a compliant silicone surface (n_3). A schematic outlining the sensor configuration is depicted in Fig. 2. Our sensor comprises an acrylic sheet (61 cm $\times$ 30.5 cm $\times$ 8 mm) that is illuminated lengthwise by high-brightness 850-nm infrared LED strips (Environmental Lights) and covered with a sheet of 3-mm thick silicone rubber (Mold Star® 15, Smooth-On™). The acrylic is embedded into a tabletop and a high-speed camera (OptiTrack S250e, Natural Point) is positioned beneath the acrylic inside a darkened enclosure to capture images of the "frustrated" light as forces are applied to the silicone surface. The application of a force brings the compliant pad into intimate contact with the top surface of the acrylic. When the size of the air gap between the compliant surface and the acrylic approaches the wavelength of the infrared light, FTIR occurs and the escaping light illuminates a spot on the compliant silicone surface, which is detected and recorded by the camera. Though the acrylic and silicone sheets each measure 61 cm $\times$ 30.5 cm, camera placement for high spatial resolution creates an active area of the sensor that is approximately 24 cm $\times$ 24 cm.

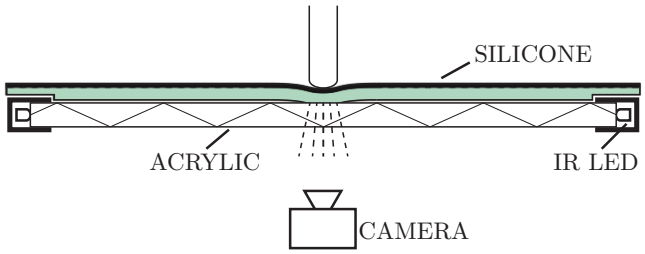

Fig. 2. The sensor is constructed by overlaying a sheet of silicone rubber on an acrylic surface that is edge-lit by high-power infrared LEDs at a wavelength of 850 nm. The light is totally internally reflected within the acrylic medium (indicated by the zigzag lines). Microscale roughness on the surface of the silicone creates a small air gap between the rubber and the acrylic. A force applied to the silicone narrows the air gap, and when the gap approaches the wavelength of the light, internal reflection is "frustrated." IR light leaving the acrylic around the point of application of the force is reflected off of the silicone and captured by a high-speed camera.

The sensor is designed to resolve ground reaction forces generated by the locomotion of small robots. For example, the dynaRoACH robot has a mass of approximately 24 g and uses a biologically-inspired alternating tripod gait. The stance phase of this gait consists of three legs nominally in simultaneous contact with the ground. During quasi-static walking, we might therefore expect average per-leg forces on the order of 80 mN. During dynamic locomotion, however, forces will be much higher, and the likelihood of having fewer than three legs in contact with the ground will increase. In the design of this sensor, we assume dynamic loads approximately 3 times greater than static loads and allow for the possibility of the entire dynamic load (750 mN) being born by a single leg of the robot. Thus, the target range of our sensor is 50 - 750 mN. The important properties of the silicones for the design of this sensor are Shore Hardness and the tendency to exude silicone oil (and leave residue on the surface of the acrylic). Initial tests of a variety of silicone rubbers demonstrated that the sensitivity to applied

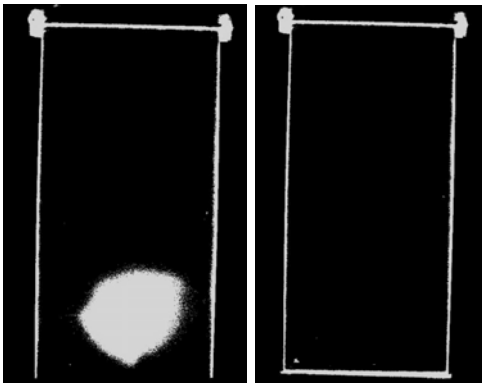

Fig. 3. A comparison of a frame of raw data from the force sensor in the motion capture arena with (left) and without (right) ambient IR illumination enabled. This initial test demonstrated the necessity of dying the the silicone layer to ensure total opacity to infrared light.

forces is inversely related to the Shore Hardness of the silicone layer. However, softer silicones are also prone to adhering to the surface (as was the case for most of the rubbers with a Shore Hardness below 10A), and they may also exude oil. This oil eliminates the air gap necessary to prevent FTIR when no force is applied to the sensor. Based on these specifications, we chose Mold Star 15 (Smooth-On) with a silicone thinner additive to attempt to optimize its Shore Hardness. The silicone layer is mixed (in liquid form) from a two-part mixture, degassed under vacuum, and poured at room temperature and pressure. To achieve the microscale roughness that creates the air gap between the silicone and the smooth acrylic surface, the silicone is poured onto and allowed to cure on a sheet of commercially available posterboard. The posterboard creates rough features on the surface of the silicone with sizes on the order of 20 - 40 μm. It may also be possible to control the sensitivity of the sensor by manipulating the roughness of either the silicone or the acrylic surface (or both).

After integrating the sensor into the motion capture arena, we discovered that the silicone was not entirely opaque to infrared light, making the force sensor readings susceptible to interference from the very bright IR illumination provided by the LEDs built into the motion capture cameras. A comparison of a frame of raw data with and without the IR illumination from the motion capture system is shown in Fig. 3. To resolve this issue, black dye was mixed into the silicone prior to curing to make it opaque to IR. However, the addition of the dye drastically decreased sensitivity of the sensor to small forces. The solution to this problem was to create a bilayer sheet with a bottom layer of undyed silicone (that contacts the acrylic surface) and a thin top layer of silicone dyed black to block the ambient IR. Pouring the top layer of the bilayer sheet before the bottom layer is fully cured enables the silicone to bond chemically across the layers, preserving continuous, uniform mechanical properties. The thickness of each layer in the bilayer sheet is controlled by controlling the volumes of the undyed and dyed silicone poured into the mold.

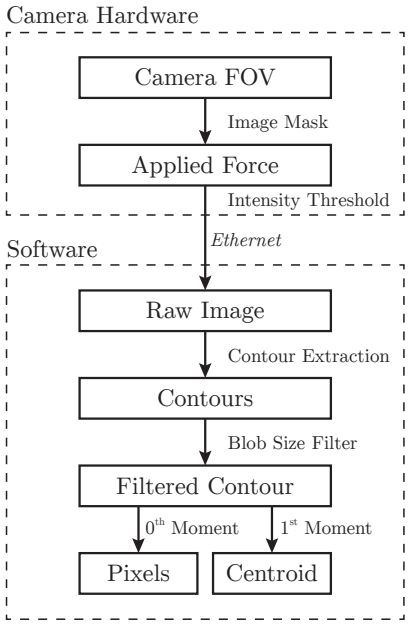

Fig. 4. A process diagram illustrating how relevant image characteristics are extracted from the raw data provided by the camera. 1) A hardware mask (implemented on the camera) filters noise. 2) An adjustable intensity threshold converts grayscale pixel values into a segmented binary image. 3) The segmented image is sent to the PC and contours are extracted using OpenCV. 4) A size filter ensures random noise is not detected as a force. 5) Image moments are used to extract the centroid of the contour (center of the applied pressure) and the area of the contour (proportional to applied force).

B. Image Processing

An important component of the sensor system is the imaging of the "frustrated" light and the processing used to extract the relevant image data, as outlined in Fig. 4. Once the relevant image characteristics are extracted, they can be converted into force data via calibration. When a force is applied to the sensor and data is captured, the resulting image is grayscale – lighter pixels represent more contact between the silicone and the acrylic and darker pixels represent less contact (or applied force). Image processing begins onboard the camera with hardware masking and intensity filtering. With extended use, the acrylic surface can become contaminated with trace amounts of oil, and it can become physically damaged resulting in nicks and scratches. Any of these effects will tend to increase noise in the image. Though it is not desirable to mask pixels inside the working area of the sensor, noisy pixels near the edges can be effectively eliminated by applying a hardware mask to prevent those pixels from being imaged. The intensity filter is then used to convert from a raw grayscale image to a binary image which is sent over the network from the camera. On the PC, OpenCV is used to extract contours. Contours are filtered by size to remove any small groupings of pixels resulting from noise. Contour size and centroid are extracted using the 0^{th} and 1^{st} image moments, respectively. Each resulting image is 832 $\times$ 832 pixels, giving the sensor a spatial resolution of approximately 0.3 mm. Programmatic control of the cameras

and integration of force sensing with motion capture data is enabled by a Python wrapper we developed for the OptiTrack Tracking Tools API using Cython [22].

III. CALIBRATION

In order to accurately estimate normal forces, it is necessary to convert the pixel data (contour area) that results from the image processing algorithm into force data (magnitude of applied normal force). The process of sensor calibration typically involves computing the solution to the overdetermined system of the form $y = \mathbf{U}b$ where $y \in \mathbb{R}^{r\times 1}$ represents measurements of the observable quantity (pixels in our case), $\mathbf{U} \in \mathbb{R}^{r\times m}$ represents sets of known applied inputs (forces in our case), and $b \in \mathbb{R}^{m\times 1}$ represents unknown parameters. The value of b that minimizes $(y - \mathbf{U}b)^{\mathsf{T}}(y - \mathbf{U}b)$ gives the best fit calibration. However, because the mechanical and optical properties of the silicone rubber can vary over the area of sensor (the impacts of which are most clearly seen in Fig. 5), it becomes necessary to compute local calibrations that provide compensation for that variation.

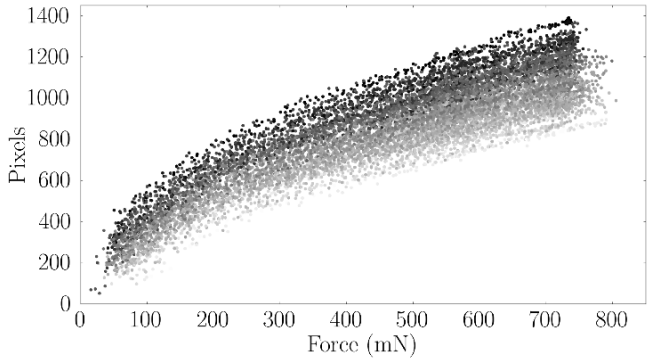

Fig. 5. Raw data resulting from the dynamic application of increasing forces to 225 equally spaced points over the entire area of the sensor. The number of pixels detected shows a logarithmic response to the applied force and varies with position of application of the force. The data points are shaded according to distance from the center of the sensor area with darker points being closer.

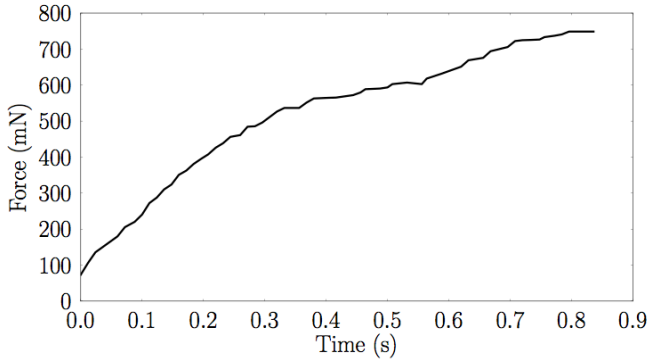

Fig. 6. A typical dynamic calibration load curve showing the time rate of application of a monotonically increasing calibration force to the sensor.

A. Method

To account for local variations in the mechanical properties of the silicone, we divide the sensor into a 14 × 14 grid and apply a sequence of known forces to points located at the corners of the 196 grid cells. The viscoelasticity of the silicone requires that the forces be applied dynamically to avoid effects of stress relaxation. A static calibration will overestimate the sensitivity of the sensor because more contact area between the silicone and the acrylic will develop over time for a constant applied force. Fig. 6 shows a typical load curve for our dynamic calibration. While it is possible to compute a local calibration curve at each of the 225 corners of the grid, we found that a simple 3-D piecewise linear interpolation of the raw calibration data, (x, y, $\log F$) produced the most accurate results. The logarithm of force was used instead of force because the log transformation approximately linearizes the pixel output as demonstrated in Fig. 7, making the linear interpolation more accurate.

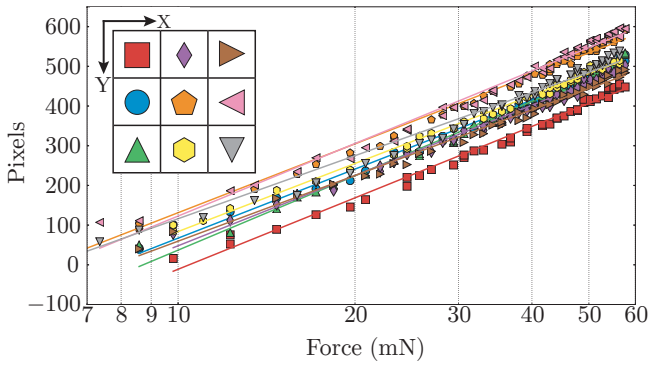

Fig. 7. Raw sample data from different regions of the sensor are shown on a semilogarithmic plot with corresponding linear fit lines. The sensor was divided into a 3×3 grid and data were collected at the center point of each grid cell. Corresponding markers are shown in the grid cells in which their respective data points were taken.

In order to systematically calibrate the working area of the sensor, we developed an automated setup that enables us to accurately and repeatably apply known forces at any location on the sensor surface. The calibration system consists of a five-axis robotic arm (R17, ST Robotics) with a remote load cell (Chatillon DGGS-R-250g) attached in place of a manipulator or end effector. A 6.35-mm diameter spherical indenter is affixed to one end of a compliant Sarrus linkage and the other end of the linkage is affixed to the input of the load cell. Though the specified spatial resolution of the R17 arm is 0.1 mm, the compliant Sarrus linkage acts as a nonlinear (softening) spring that enables us to translate relatively large displacements into relatively small forces. At each point in the calibration grid a continuously increasing force is applied, images from the sensor's camera are captured, and readings from the load cell are recorded. Because this system enables dynamic calibration, a full calibration routine can be run over the entire sensor in less than ten minutes. Fig. 8 is a photo of the calibration setup used in our experiments.

B. Results

Fig. 9 depicts the percentage errors resulting from applying the calibration to approximately 200 randomly chosen

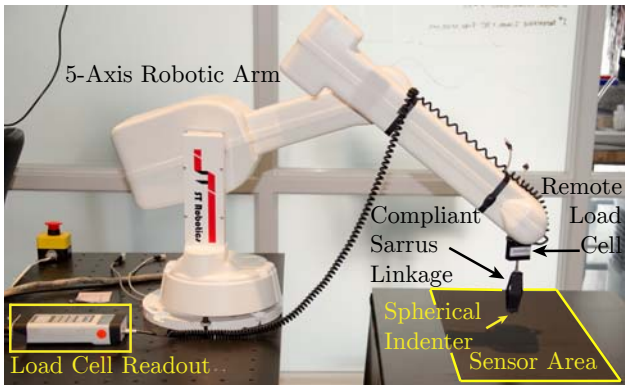

Fig. 8. A photograph depicting the hardware setup used to generate calibration data for the sensor. A remote load cell is attached to a five-axis robot arm and used to apply known forces over the surface of the sensor. Control is provided by a PC which simultaneously commands the arm, reads from the remote load cell, and processes image data received from the multi-touch sensor's camera.

forces applied at random locations over the sensor's surface. Using this calibration approach, we are able to achieve measurement error of less than 1%. In the upper half of the range of applied forces the error is consistently very low. However, at low forces, the variance in the error is much higher. Applied forces below 50 mN were culled from these data sets because quantization effects from both the tactile sensor as well as the load cell and the robotic arm created noisy, inconsistent data.

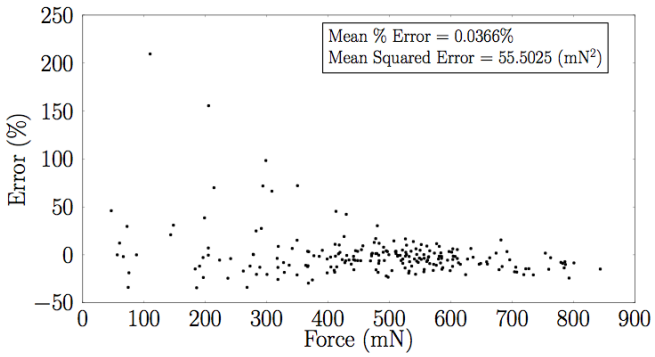

Fig. 9. Estimation error for approximately 200 randomly chosen forces applied at random locations on the sensor.

IV. VALIDATION

One major advantage of the approach taken in this work is the integration of high-speed, high-resolution, large-area, tactile force sensing with motion capture to provide more complete dynamic state information for small, highly dynamic systems. To demonstrate integration of these sensing techniques, we designed a validation experiment to test the dynamic force response of the sensor and synchronization of force and motion data capture.

A. Method

The simplest validation experiment consists of a single object tracked in the motion capture arena while simultaneously applying a normal force to the sensor. Motion capture data is used to estimate the acceleration (in the vertical direction) of the object providing the right-hand side (ma) of Newton's Second Law. The force sensor provides an estimate of the reaction force applied by the sensor to the object, and if the two estimates are consistent for the times when the body is in contact with the sensor, it can validate the dynamic performance of the force sensor.

Using this approach, we demonstrate the capability of the sensor to provide reaction force data synchronized with motion capture estimates. We drop a 1-g ball from a height of approximately 30 cm onto the sensor. Its trajectory is tracked using four motion capture cameras through all stages of its motion: drop, initial collision with the table, and subsequent bounces. Force data captured by the tactile sensor and position estimates provided by the additional four motion capture cameras are shown in Fig. 10

TABLE I

RESULTS OF COMPARISON OF REACTION FORCE ESTIMATES USING MOTION CAPTURE AND THE TACTILE SENSOR

Time	Force estimated using motion capture (mN)	Force measured by sensor (mN)	% Error
0.924	840	650	22.6
1.276	577	550	4.7
1.516	330	476	41
1.688	272	251	7.7
1.816	192	181	5.7
1.916	117	123	5

B. Results

To validate the performance of the sensor, we estimated the peak reaction forces at the times corresponding to the six peaks shown in Fig. 10. Peak accelerations were determined by simply numerically differentiating the vertical position data for the ball. Though this method tends to be noisy, the acceleration peaks created by contact with the sensor are still an order of magnitude larger than the noise created by numeric differentiation. Newton's Second Law is applied using the peak accelerations and the 1-g mass of the ball to estimate the peak reaction forces. Using the calibration procedure described in Section III, a corresponding estimate of normal ground reaction force is produced by the sensor. A comparison of the forces estimated using each method is shown in Table I.

The achievable accuracy with the ball drop can be high, but there is large variation in measurement error. It is not yet clear whether the variation is inherent to the sensor hardware or if our calibration method is insufficient to estimate reaction forces with high frequency content as is the case with the rigid bouncing ball. Calibrating for a spectrum of input frequencies is an area of further exploration.

V. CONCLUSIONS AND FUTURE WORK

We have presented a novel, high-speed, large-area, tactile force sensor appropriate for measuring normal ground reaction forces generated by small-scale legged robots. The

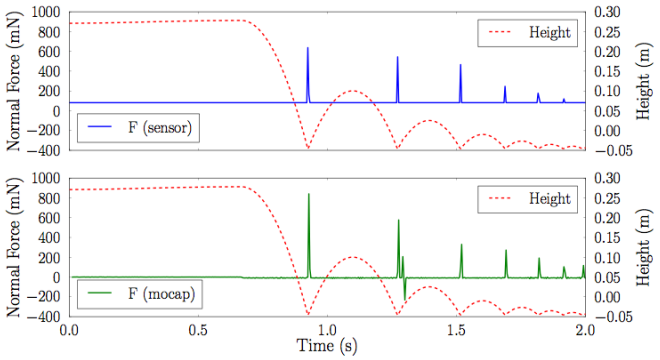

Fig. 10. A simple experiment demonstrates integration of multi-camera motion capture with ground reaction normal force sensing. A 1-g ball is dropped from a height of approximately 30 cm. Vertical position of the ball and the normal reaction force applied to the ball by the sensor are tracked and synchronized. The upper figure shows estimates of ground reaction force using the tactile sensor. The smallest value of force is not zero in this case because the calibration data excludes forces smaller than 5g due to quantization noise. The lower figure shows estimates of force resulting from twice differentiating motion capture position data to estimate vertical acceleration and, in combination with the ball's mass, applied vertical force.

system provides normal force sensing in the range of 50 - 1000 mN at a rate of 250 Hz with the ability to synchronize directly with a commercial motion capture system. Using the system we have demonstrated the ability to sense multiple small forces to a mean accuracy within 1% while simultaneously capturing estimates of kinematic state data like positions of rigid bodies.

Future work will involve improving the sensitivity and accuracy of the sensor through the optimization of compliant material properties, sensor geometry, and surface treatments for the acrylic. For example, laser etching the acrylic may allow for more precise control of surface roughness, potentially improving sensitivity while dynamic mechanical analysis of the silicone will allow us to create a material model that accounts for the hysteretic effect of stress relaxation on contact area measurements. A more complete understanding of the role of material and surface properties in performance will enable us to parameterize the design so that it may be scaled up to measure, for example, human-scale forces (like those resulting from walking) or scaled down to measure individual ground reaction forces generated by insects or small lizards as well as robots. Finally, further work is necessary to understand and calibrate out sources of noise that have potential to create significant measurement error.

ACKNOWLEDGMENTS

We would like to thank Professors David Barrett and Andrew Bennett for providing access to the robotic arm. We would also like to thank Professor Bradley Minch for his insightful comments and helpful feedback. Aaron Hoover would like to thank Sam Burden for thought-provoking discussions of calibration and data-fitting.

REFERENCES

[1] A. M. Hoover, E. Steltz, and R. S. Fearing, "RoACH: An autonomous 2.4g crawling hexapod robot," in *IEEE Int. Conf. on Intelligent Robots and Systems*, Nice, France, Sept. 2008.

[2] A. M. Hoover, S. Burden, X. Y. Fu, S. S. Sastry, and R. S. Fearing, "Bio-inspired design and dynamic maneuverability of a minimally actuated six-legged robot," in *IEEE Int. Conf. on Biomedical Robotics and Biomechatronics (BioRob)*, 2010, pp. 869–876.

[3] P. Birkmeyer, K. Peterson, and R. S. Fearing, "Dash: A dynamic 16g hexapedal robot," in *IEEE Int. Conf. on Intelligent Robots and Systems*, St. Louis, MO, 2009.

[4] A. T. Baisch, P. S. Sreetharan, and R. J. Wood, "Biologically-inspired locomotion of a 2g hexapedal robot," in *Intl Conf on Intelligent Robots and Systems*, 2011.

[5] J.-M. Mongeau, B. McRae, A. Jusufi, P. Birkmeyer, A. M. Hoover, R. Fearing, and R. J. Full, "Rapid inversion: Running animals and robots swing like a pendulum under ledges," *PLoS ONE*, vol. 7, no. 6, p. e38003, 06 2012. [Online]. Available: http://dx.doi.org/10.1371%2Fjournal.pone.0038003

[6] F. Qian, T. Zhang, chen Li, A. Hoover, P. Masarati, P. Birkmeyer, A. Pullin, R. Fearing, and D. Goldman, "Walking and running on yielding and fluidizing ground," in *Proceedings of Robotics: Science and Systems*, Sydney, Australia, July 2012.

[7] C. Li, P. B. Umbanhowar, H. Komsuoglu, D. E. Koditschek, and D. I. Goldman, "Sensitive dependence of the motion of a legged robot on granular media," *Proceedings of the National Academy of Sciences*, vol. 106, no. 9, pp. 3029–3034, 2009. [Online]. Available: http://www.pnas.org/content/106/9/3029.abstract

[8] P. Birkmeyer, A. G. Gillies, and R. S. Fearing, "Clash: Climbing vertical loose cloth," in *Intelligent Robots and Systems (IROS), 2011 IEEE/RSJ International Conference on*, sept. 2011, pp. 5087 –5093.

[9] U. Saranli, M. Buehler, and D. E. Koditschek, "RHex: A simple and highly mobile hexapod robot," *The Int. J. of Robotics Research*, vol. 20, no. 7, pp. 616–631, 2001.

[10] A. Saunders, D. I. Goldman, R. J. Full, and M. Buehler, "The RiSE climbing robot: body and leg design," in *Society of Photo-Optical Instrumentation Engineers (SPIE) Conference Series*, ser. Society of Photo-Optical Instrumentation Engineers (SPIE) Conference Series, vol. 6230, Jun. 2006.

[11] J. T. Manter, "The dynamics of quadrupedal walking," *Journal of Experimental Biology*, vol. 15, no. 4, pp. 522–540, 1938. [Online]. Available: http://jeb.biologists.org/content/15/4/522.abstract

[12] J. Harris and H. Ghiradella, "The forces exerted on the substrate by walking and stationary crickets," *The Journal of Experimental Biology*, vol. 85, no. 1, pp. 263–279, 1980. [Online]. Available: http://jeb.biologists.org/content/85/1/263.abstract

[13] R. J. Full, A. Yamauchi, and D. Jindrich, "Maximum single leg force production: cockroaches righting on photoelastic gelatin," *J Exp Biol*, vol. 198, no. 12, pp. 2441–2452, 1995. [Online]. Available: http://jeb.biologists.org/cgi/content/abstract/198/12/2441

[14] Z. Dai, Z. Wang, and A. Ji, "Dynamics of gecko locomotion: a force-measuring array to measure 3d reaction forces," *The Journal of Experimental Biology*, vol. 214, no. 5, pp. 703–708, 2011. [Online]. Available: http://jeb.biologists.org/content/214/5/703.abstract

[15] R. Boie, "Capacitive impedance readout tactile image sensor," in *Robotics and Automation. Proceedings. 1984 IEEE International Conference on*, vol. 1, mar 1984, pp. 370 – 378.

[16] I. Rosenberg and K. Perlin, "The unmousepad: an interpolating multi-touch force-sensing input pad," *ACM Trans. Graph.*, vol. 28, no. 3, pp. 65:1–65:9, Jul. 2009. [Online]. Available: http://doi.acm.org/10.1145/1531326.1531371

[17] J. Y. Han, "Low-cost multi-touch sensing through frustrated total internal reflection," in *Proceedings of the 18th annual ACM symposium on User interface software and technology*, ser. UIST '05. New York, NY, USA: ACM, 2005, pp. 115–118. [Online]. Available: http://doi.acm.org/10.1145/1095034.1095054

[18] J. Smith, T. Graham, D. Holman, and J. Borchers, "Low-cost malleable surfaces with multi-touch pressure sensitivity," in *Horizontal Interactive Human-Computer Systems, 2007. TABLETOP '07. Second Annual IEEE International Workshop on*, oct. 2007, pp. 205 –208.

[19] [Online]. Available: http://naturalpoint.com

[20] [Online]. Available: http://www.vicon.com

[21] S. Zhu, A. W. Yu, D. Hawley, and R. Roy, "Frustrated total internal reflection: A demonstration and review," *American Journal of Physics*, vol. 54, no. 7, pp. 601–607, 1986. [Online]. Available: http://link.aip.org/link/?AJP/54/601/1

[22] [Online]. Available: http://www.cython.org/